Electrochemical Deposition of Organic Semiconductors on High Surface Area Electrodes for Solar Cells

ARTICLE *in* THE JOURNAL OF PHYSICAL CHEMISTRY B · OCTOBER 2000

Impact Factor: 3.3 · DOI: 10.1021/jp001926w

Journal of The Electrochemical Society, **148** (11) C709-C714 (2001)
0013-4651/2001/148(11)/C709/6/$7.00 © The Electrochemical Society, Inc.

Electrochemical Deposition of Organic Semiconductors

The Method, Mechanism, and Critical Deposition Parameters

Yishay Diamant and Arie Zaban*,z

Department of Chemistry, Bar-Ilan University, Ramat-Gan 52900, Israel

Electrochemical deposition of the organic semiconductor perylene phenethylimide (PPEI) is reported. The deposition is based on neutralization of the unstable PPEI ions that are produced electrochemically during the deposition process. A mechanism for the deposition is suggested based on a comparison between depositions in the dark and under illumination. A thin insolating layer of PPEI is first formed followed by growth into long crystals via localized conductive points. The nature and the quantity of the conductive points are determined at the beginning of the deposition which was found to be the most sensitive part of the process.
 [DOI: 10.1149/1.1405517]

Manuscript submitted April 12, 2001; revised manuscript received June 13, 2001. Available electronically September 20, 2001.

Organic semiconductors (OSCs) are the subject of an increasing number of studies because of their low cost, photochemical stability, and high absorption coefficient. The prospect that we will be able to optimize their physical properties by synthetic methods for specific applications gives further motivation.[1,2] OSCs can be used for applications such as light emitting diodes,[3-5] photoconductors,[6] chemical sensors,[6,7] and bilayer organic solar cells.[8-12] However, OSC-based photovoltaic cells have shown a low efficiency of solar energy conversion.[8-14] One of the major reasons for this inefficiency is the high resistivity of these photovoltaic materials to charge migration, which limits the thickness of the OSC layer that can be used.[8,15-18] This limitation results in a low optical density and thus, in a low conversion efficiency of the solar cell.

In order to overcome this limitation, we developed a new method for the deposition of OSC. This method results in the formation of a thin layer on porous substrates. In contrast to the standard deposition method, evaporation in a high vacuum, by using the new method it is possible to deposit OSCs into a high surface area, nanoporous substrate.[19] Correspondingly, the optical density increases without thickening the OSC layer. The method is based on the electrochemical deposition of OSC ions that are electrochemically produced during the deposition process. This unique procedure is required because of two factors: one, the insolubility of the OSCs unless they are ionized, and two, the short lifetime of the ions.[20,21] Using the new deposition method, we were able to control properties such as crystal structure, size, and orientation of the deposited OSC.[22,23] The process is performed under ambient conditions and, thus, it is superior to the evaporation in a high vacuum, because our method does not require high temperatures that can decompose the material.[6,22]

In our previous paper,[24] we reported on a solar cell which was based on this electrodeposition. The solar cell consisted of a nanoporous electrode in which a high surface area, TiO_2 sintered on a conducting glass, served as the substrate. Into this porous electrode, we deposited a layer of OSC, perylene phenethylimide (PPEI) (see inset Fig. 2). The electrolyte I^-/I_3^- redox couple served as a liquid quencher and a Pt-coated F-doped SnO_2 film was used as a counter electrode. This solar cell showed that the electrodeposition is applicable for solar energy conversion devices, and the cell is suitable for other applications. Furthermore, the ability to control the deposited OSC properties by deposition parameters makes this electrodeposition process important for many OSC-based applications. In this paper, we provide a more comprehensive study of the new deposition method describing the electrochemical processes and the parameters that affect the layer properties. This study was conducted using flat electrodes in order to achieve a better understanding of the deposition processes. The most important parameter was found to be illumination, *i.e.*, performing the deposition either in the dark or under illumination. We also studied the following parameters: the type of the supporting electrolyte, the electrolyte concentration, the potential of the target electrode, and the distance between the target and the source electrodes. All of these parameters were found to influence the deposition result.

* Electrochemical Society Active Member.
z E-mail: zabana@mail.biu.ac.il

Experimental

Electrochemical deposition.—Perylene phenethylimide (PPEI) from SynTec was used as received. The conducting glass (Hartford Glass, 8 Ω/□ F-doped SnO_2) was washed with water and soap, soaked for 10 min in HF solution (1:40 mixture of HF analytic:H_2O), washed again with deionized water, and then dried in a nitrogen stream. The electrochemical deposition was performed in a dry nitrogen glove box (<1 ppm H_2O and O_2) using a battery-grade dry electrolyte. The electrolyte solution consisted of 0.4 M $TBAClO_4$ (tetrabutylammonium perchlorate) in dry acetonitrile. The electrochemical cell consisted of four electrodes. The source and the target electrodes were conducting glass with surface areas of 0.196 and 0.07 cm^2, respectively. The reference electrode was $Ag/AgNO_3$, and the counter electrode was a platinum wire. All potentials are reported *vs.* the reference; $Ag/AgNO_3$ electrode which is 0.1 V negative of ferrocene/ferrocenium (Fe^0/Fe^+). Both the reduction of the PPEI from the source electrode by cyclic voltammetry and the oxidation under constant potential on the target electrode were controlled by a bipotentiostat (Eco Chemie Autolab 20). For electrodeposition under illumination, a 488 nm line from an argon laser was used.

Spectroelectrochemistry.—The spectroelectrochemical reduction was performed under dry conditions using a sealed cell that was loaded in the nitrogen atmosphere glove box. This measurement employed a three-electrode configuration. The electrolyte solution was 0.4 M $LiClO_4$ or 0.4 M $TBAClO_4$ in dry acetonitrile. The reference electrode was a silver wire, which was calibrated *vs.* $Ag/AgNO_3$. The absorption spectra were measured with a HP 8453 spectrophotometer.

Instruments.—Fluorescence measurements were conducted using an SLM Aminco series 2 spectrofluorometer. The excitation wavelength was 460 nm. Lateral fluorescence imaging was performed in SpectraCube SD-200 (Applied Spectral Imaging, Migdal HaEmek, Israel). Scanning electron microscopy (SEM) micrographs were taken with a JSM-840 (JEOL, Japan).

Impedance spectroscopy was measured by a frequency response analyzer (FRA, Eco Chemie Autolab 20), using a three-electrode cell. The working electrode was the conducting glass covered with the electrodeposited PPEI (surface area of 0.07 cm^2). An $Ag/AgNO_3$ electrode was used as a reference, and a platinum wire served as a counter electrode. The electrolyte consisted of 15 mM ferrocene/ferrocenium (Fe^0/Fe^+) as a redox couple and 0.4 M $TBAClO_4$ as a supporting electrolyte in acetonitrile.

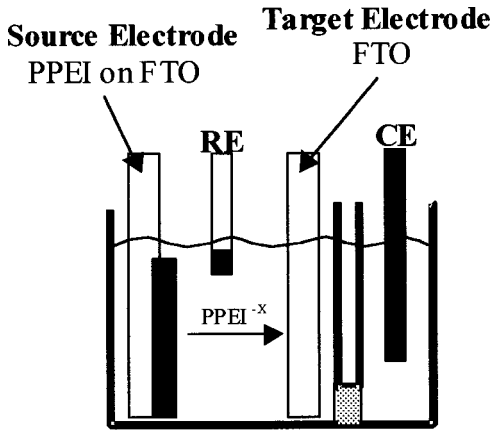

Figure 1. The electrodeposition cell. The PPEI is desorbed (reduced) from the source by cyclic voltammetry and deposited (oxidized) on the target under constant positive potential.

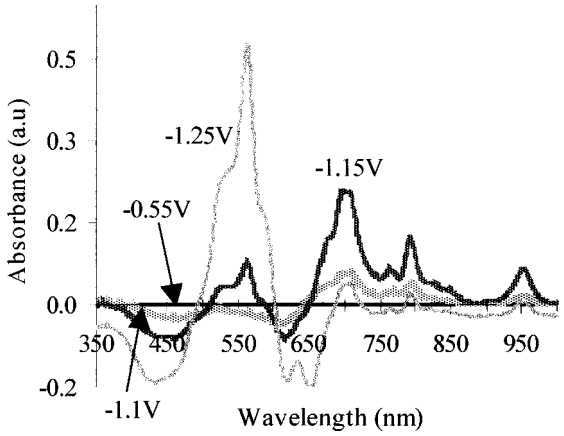

Figure 3. Spectroelectrochemical measurement of the solution near the source electrode during the reduction process. Presented are the radical anion spectrum characterized by peaks at 710, 795, and 960 nm measured at −1.15, and the dianion spectrum having peaks at 540 and 565 nm measured at −1.25. The absorbance at the open-circuit voltage served as a baseline.

Results and Discussion

Like most OSCs, the PPEI is insoluble in many solvents unless it is ionized.[20,21] Therefore, the electrochemical deposition is based on the neutralization of perylene ions that are produced *in situ* by electrochemical reduction. In practice, we used a bipotentiostat that controlled two working electrodes (Fig. 1). The PPEI, spread by shear force on one of the working electrodes denoted as the source, was reduced during cyclic voltammetry. The PPEI was then oxidized (neutralized), under a constant positive potential, on the other working electrode denoted target.

We first discuss the ionization process that occurs at the source electrode. Figure 2 presents a cyclic voltammetry of the reduction process, showing two reductions to the PPEI radical anion starting at −1.03 V and to the PPEI dianion at −1.16 V. The formation of the radical anion and the dianion is also evident from spectroelectrochemical measurements. Figure 3 shows the spectra of the solution measured during the reduction process. Both the radical anion and the dianion have a unique spectrum that differs significantly from that of the neutralized PPEI. The radical anion spectrum, characterized by peaks at 710, 795, and 960 nm,[21] was measured at −1.15 V. The dianion spectrum having peaks at 540 and 565 nm[21] was measured at −1.25 V. Figure 4 shows the intensity of the solution spectra at the wavelengths of the radical anion (710 nm) and the dianion (565 nm) as a function of the applied potential. The current onset during the CV correlates well with the onset of the absorption at 710 nm, which corresponds to the radical anion. In the potential range from −1.1225 to −1.125 V, both the radical anion and the dianion are produced. The bleaching of the intensity at more negative potentials is a consequence of the ions' instability and their dilution in the cell volume.

The ability to create the ions is feasible only if the supporting electrolyte consists of $TBAClO_4$. Isolated ions were not produced in experiments that were conducted with a supporting electrolyte consisting of $LiClO_4$. The reasons for this behavior may be due to the following factors: the production of stable particles of the form $PPEI_xLi_y$ which are formed during intercalation of Li^+ and/or the inability of the small Li^+ to stabilize the PPEI ions which therefore neutralize immediately in solution. However, a comprehensive investigation of these speculations is beyond the scope of this work.

In summary, it is possible to ionize and thus dissolve the PPEI for a limited period of time in a $TBAClO_4$-based solution.

In a typical deposition process, the ions are anodically neutralized on the target electrode in parallel to the ionization (reduction) process. Figure 5 shows a typical electrodeposition process, the re-

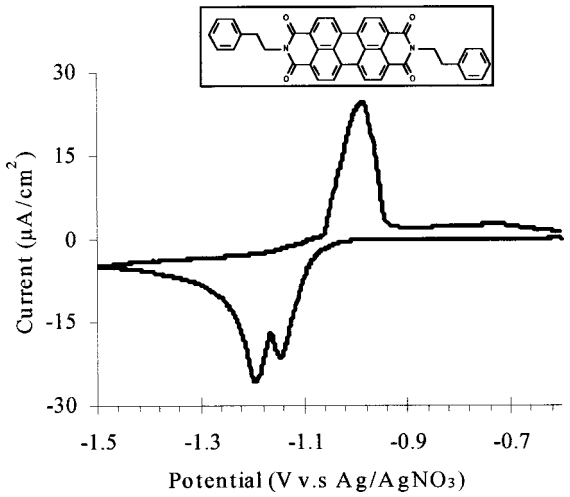

Figure 2. Cyclic voltammetry of the reduction (desorption) process at the source electrode. The two reduction peaks correspond to the formation of the radical anion and dianion. The electrolyte solution consisted of 0.4 M $TBAClO_4$ in acetonitrile. The structure of PPEI is presented in the inset.

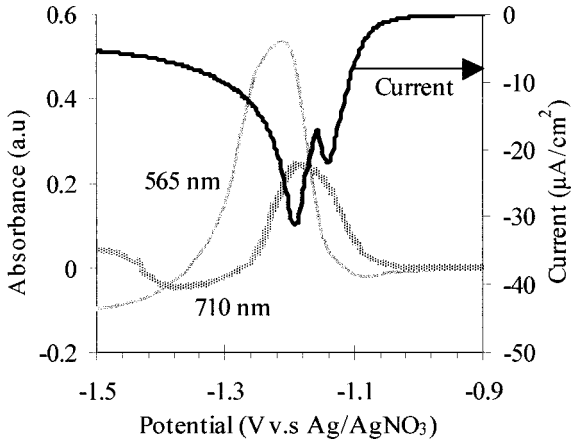

Figure 4. The absorption of the solution at 565 and 710 nm and the source electrode current as a function of potential, showing a correlation between the current shape and the formation of the radical anion (710 nm) and dianion (565 nm).

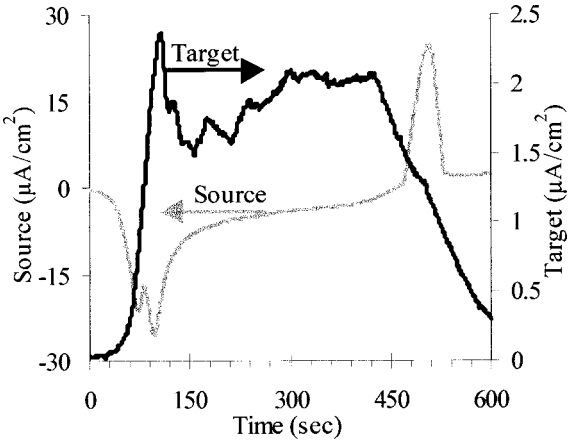

Figure 5. A typical electrodeposition process. The reduction of the PPEI from the source electrode and its oxidation on the target electrode, as a function of the time.

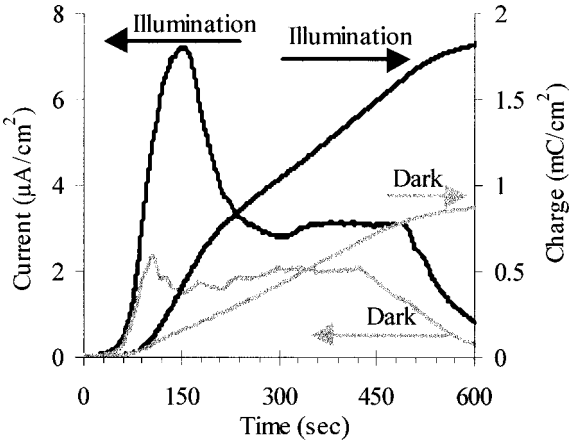

Figure 7. The deposition current and accumulated charge of the target electrode under 488 nm illumination and in the dark. Illumination leads to higher deposition current and consequently higher collected charge.

duction of the PPEI from the source electrode by cyclic voltammetry (black) and the neutralization of the ions on the target electrode under a constant potential (gray). Figure 6 shows that the deposited PPEI has absorption and emission spectra similar to that of crystalline PPEI prepared by other methods.[20,21,25,26] This means that the deposited PPEI has a crystalline structure. The formation of the crystal structure can be explained by two mechanisms. One is that PPEI is deposited on the conducting glass as an amorphous layer, which then crystallizes due to the electrolyte's presence. The solvent provides the necessary condition for the reorganization to the crystal structure.[21,23,25] The second mechanism is the ions are neutralized on the conducting glass in a crystal structure. In other words, an amorphous phase is not formed during the deposition. As is discussed below, the second option apparently describes the process better, *i.e.*, the ions are deposited into a crystal structure. As mentioned above, the conductivity of the PPEI is low, and thus it is expected to affect the deposition process. It is expected that the resistance increases up to the complete blocking of the surface as the thickness of the PPEI layer increases. One of the ways to overcome this limitation is through the illumination of the PPEI layer during the deposition. However, this illumination process can have other effects on the resulting layer in addition to producing a thicker layer by reducing the PPEI resistivity.

In both light and dark measurements the behavior of the source electrode was similar, as evident from the shape of the dissolution

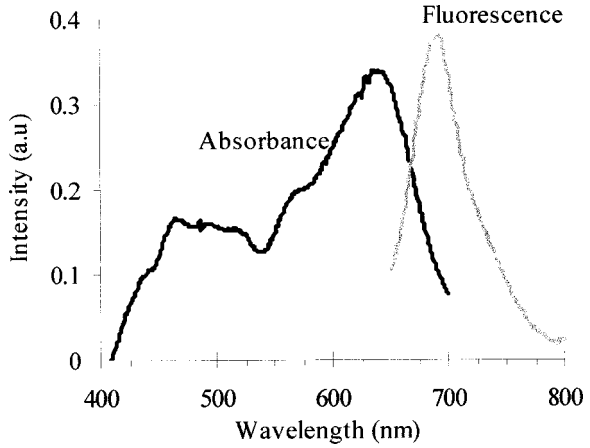

Figure 6. Absorbance and emission spectra of the deposited PPEI. The excitation wavelength is 460 nm. These spectra are similar to those of crystalline PPEI.

cyclic voltammetries. This similarity is due to the illumination path that strikes the source electrode from the solution side, so that the light is absorbed at the first 300-400 nm outer part of the film. The illumination effect is therefore distant from the substrate. Figure 7 shows the electrochemical characteristics of PPEI deposition on a target electrode during illumination at 488 nm. For comparison, we present a deposition in the dark under similar conditions. Figure 7 clearly shows that illumination leads to a higher deposition current and consequently, the charge passing through the target electrode is higher. This higher charge indicates that under illumination, the amount of the deposited material is greater, assuming that the fraction of the inefficient charge is similar in both cases. Figure 8 presents typical SEM pictures of the deposited material both under illumination and in darkness. In these two cases, large elongated crystals are deposited. These crystals have dimensions of *ca.* 0.5 μm by 5-10 μm. We assume from the electrochemical values obtained when the target electrode is illuminated that the amount of the deposited PPEI is greater and the crystals are longer. Furthermore, the SEM pictures show that the crystals grow from specific points on the substrate. Under illumination, the needle-like crystals grow from these points in all directions. The nonuniform growth at the electrode surface may result from current distribution limitations that drive the ions to the points where material was already deposited. However, this process seems inappropriate in the case of PPEI deposition due to the large resistance of the deposited PPEI. This resistance should lead to deposition at the more conducting sites in which less material was deposited, forming a homogeneous layer. A more appropriate interpretation of the SEM pictures may be that a blocking layer is first deposited on the electrode followed by growth via "weak" points in the layer. This growth probably occurs via the conducting path in the PPEI crystals, which is known to be anisotropic with respect to conductivity.[27] Such a growth may result in a needle-shape of the crystals as shown in Fig. 8. This mechanism requires that a blocking layer of PPEI be present throughout the electrode. If such a layer is thin and homogeneous, it is not likely to be observed in the SEM pictures. However, we expect to detect such a layer using lateral fluorescence imaging. Figure 9a shows this imaging of the dark deposition, indicating that there is fluorescence from the entire surface, even in areas without needles. Figure 9b shows the fluorescence spectra of the marked points in Fig. 9a, showing that although there is less material in the open areas, their spectra is similar to that of the PPEI. This observation means that there is a thin layer on the conducting glass.

At this time, we do not have direct evidence of the nature of these weak points. There can be many reasons for the formation of defects during such a deposition. For example, these defects may be caused by the trapping of the positive ions or by an orientation of

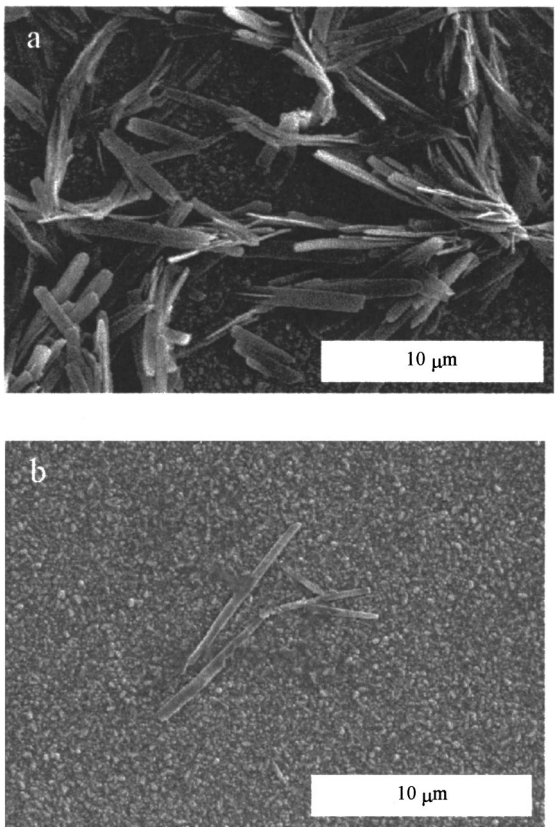

Figure 8. SEM pictures of the deposited PPEI under (a) 488 illumination (b) dark conditions. As shown, large elongated crystals are deposited. Under illumination, the amount of the PPEI is larger and the crystals are longer.

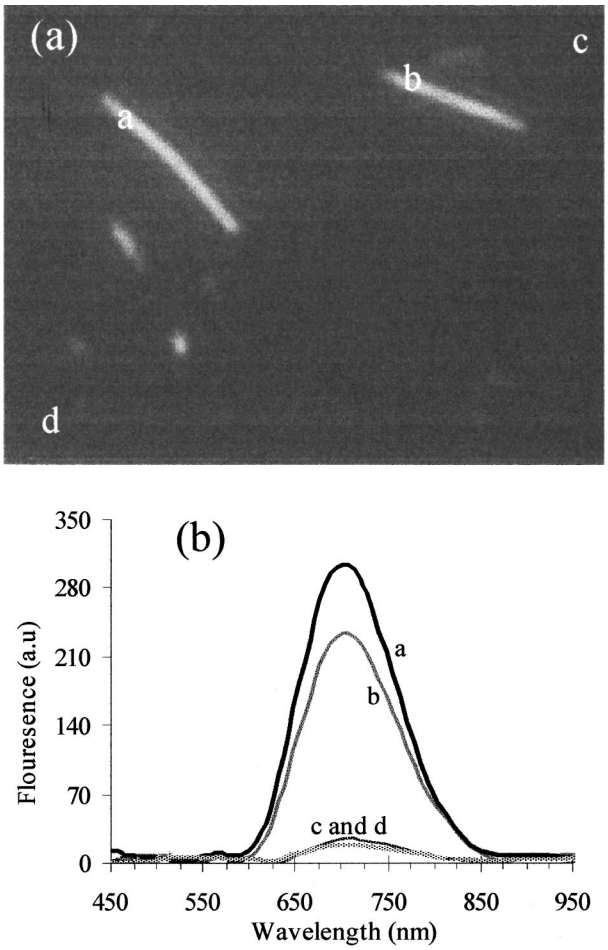

Figure 9. Lateral fluorescence imagining of the deposited PPEI in the dark (a) and fluorescence spectra of the marked points (b). All the surface including areas without needles exhibits some fluorescence.

the molecules. The following is a description of two measurements impedance spectroscopy and illumination modulation, that provide some insight regarding the defects. The impedance measurements were performed immediately after the electrodeposition in dry conditions and after exposure to ambient air. The conducting glass covered with the electrodeposited PPEI served as a working electrode and ferrocene/ferrocenium (Fe^0/Fe^+) as a redox couple. As noted in Fig. 10, these measurements show that the resistance of the PPEI electrode increases after exposure to air. This increasing resistance is attributed to a modification of the defects by humidity. Additional information regarding these defects is provided by the following two experiments. One, electrodeposition of PPEI which began under illumination of the target electrode for a limited time; the remainder of the process was performed in the dark. Two, a deposition starting under limited-time dark conditions followed by illumination. These experiments show that only the conditions which occur during the first few seconds influence the deposited material. In other words, extinguishing the illumination during the deposition did not affect the amount of charge deposited, in comparison to illumination which occurred throughout the deposition. Similarly, when the deposition began in the dark, the illumination did not affect the deposition which resembled the deposition performed in the dark. Our results apparently indicate that the illumination increases the formation of the defects. Therefore, when the electrodeposition begins under illumination, the first blocking layer has more weak points that lead to more deposition. To summarize, our results show that a thin layer is first deposited on the conducting glass and then the electrodeposition proceeds from weak points in this layer. The exact nature of the points is unclear, however one can describe them as defects in the PPEI crystal.

Unlike ordinary electrochemistry, in this electrochemical deposition, there are no electroactive species in the solution at the beginning of the process. Furthermore, the production rates of these species vary and their type changes from radical anion or dianion throughout the process (Fig. 2). In addition, the ionized species are produced on one working electrode, and they must pass some distance in order to neutralize on the other working electrode. The dual

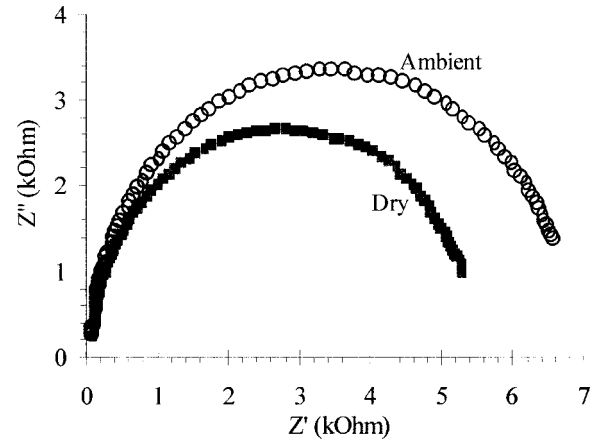

Figure 10. Impedance spectra of the target electrode after deposition under dry conditions and after the exposure to ambient air. The resistance increases after the exposure to air. Ferrocene/ferrocenium (Fe^0/Fe^+) served as a redox couple.

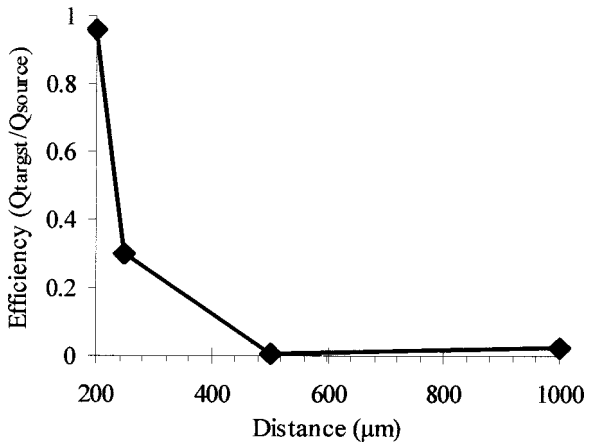

Figure 11. The efficiency of the deposition process under illumination as a function of the distance between the source and target electrodes. The efficiency is the ratio between the charge collected on the target and the charge produce by the source.

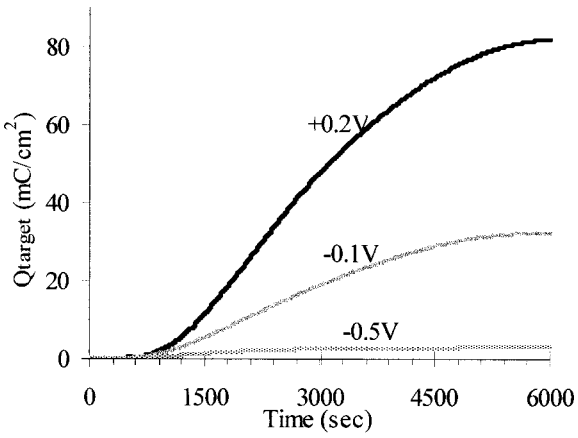

Figure 12. The deposition charge at the target electrode under different applied potentials while the target electrode is illuminated. All potentials are more positive than the redox potential of the PPEI ions.

motivation for the ion motion includes migration, derived from the electric field, and diffusion derived from the concentration gradient. In other words, the concentration of the ions is zero until their dissolution begins at the source electrode. After their dissolution, the ions' front moves under the influence of the electric field and the concentration gradient. It is also important to consider the short lifetime of the ions. In order to successfully deposit the PPEI, the ions must reach the target electrode before they neutralize in the solution. Thus, we must ensure that the ions' lifetime is not shorter than their transport time. To describe this behavior, we investigated three parameters: one, the distance between the source and the target electrodes; two, the oxidation potential at the target electrode; and three, the concentration of the supporting electrolyte. These parameters affect the migration, diffusion, and thus the transport time of the ions to the target electrode. However, the system is too complicated for a comprehensive quantitative description. But, the results correlate qualitatively with this description of the deposition process.

The distance between the source and the target electrodes.—Teflon spacers with different widths were used to set the distance between the two electrodes. The dissolution charge measured at the source electrode varied up to 7% between the different experiments. Figure 11 presents the efficiency of the deposition as a function of the distance. The efficiency is defined as the ratio between the total charge used to collect the PPEI on the target electrode divided by the total charge needed to produce the PPEI ions at the source electrode. When the distance between the electrodes increases, the oxidation current on the target electrode reduces significantly. As a result, the deposition efficiency drops to approximately 0 at 500 μm distance (Fig. 11). The significant drop in efficiency is a consequence of three factors. One is the short lifetime of the PPEI ions. After the ions were produced by the source electrode, they must move toward the target electrode in order to be deposited. When the distance increases, the transport time also increases and thus the amount of the PPEI ions available at the target electrode decreases. Specifically, if the transit time between the electrodes is longer than the PPEI ions' lifetime, then the ions neutralize in the solution. A second factor is the migration rate of the ions. The negative ions are attracted by the positive electric field that is created in the target electrode. If the distance extends beyond the main potential drop area which depends on various parameters (discussed below), then the migration rate will be slow. Under such conditions, the ions' transport time to the target electrode is longer than their lifetime. The third mechanism is the diffusion rate of the ions. The ions' motion is also influenced by the concentration gradient. Since the ion concentrations at the source and target electrodes are not affected by the distance between them, the concentration gradient becomes less steep as this distance increases. Consequently, at greater distances between the electrodes, the ions' motion is slower and thus the deposition efficiency drops to nearly zero.

Based on the time differences between the onset of the ionization and the onset of the neutralization, we were able to calculate the mean velocity of the radical ions: 15 and 7 μm/s for 200 and 250 μm distances, respectively. At both 500 and 1000 μm distances, the velocity is even slower, but we cannot determine the precise velocity due to the low deposition current. The following measurements were performed using a distance of 200 μm at which the efficiency is 100%.

The oxidation potential at the target electrode.—All of the oxidation potentials applied to the target electrode were more positive than the redox potential of the PPEI ions. Thus, these experiments were performed under mass-transfer control rather than activation control. Figure 12 shows the accumulated deposition charge at three different anodic biases. As the applied overpotential is made more positive, the deposition charge increases, showing that more material was deposited. Since the process occurs beyond activation control, this can be attributed to the different electric fields induced by the different biases. This means that the more positive the potential, the more the field is extended into solution. This attracts the negative ions that are produced at the source electrode more efficiently. Consequently, the velocity of the ions should be higher, resulting in a lower transport time. In parallel, one should consider another effect of the anodic bias which is related to the high resistivity of the PPEI. Even under illumination, the resistance of the PPEI layer grows as it becomes thicker. The potential drop across the PPEI layer decreases the effective potential at the PPEI/solution interface where the ions are deposited. As the film becomes thicker, thus increasing the film resistance, the effective potential is expected to reach a limiting value that is not sufficient for further deposition. Indeed, the accumulated charge and the deposition efficiency increase when the overpotential is higher. We could not measure the influence of the film resistance exclusively. However, we could demonstrate the migration affect by measuring the influence of supporting electrolyte concentration.

The concentration of the supporting electrolyte.—The concentration of the supporting electrolyte, $TBAClO_4$, varied from 0.2 to 0.8 M. Figure 13 presents the collected charge at different concentrations showing that a lower concentration leads to a higher deposition charge. The effect of the supporting electrolyte may be attributed to its role in the determination of the profile of the electric field which is generated at the target electrode. In other words, increasing the electrolyte concentration is expected to screen the applied potential at a shorter distance from the target electrode, thus decreasing the

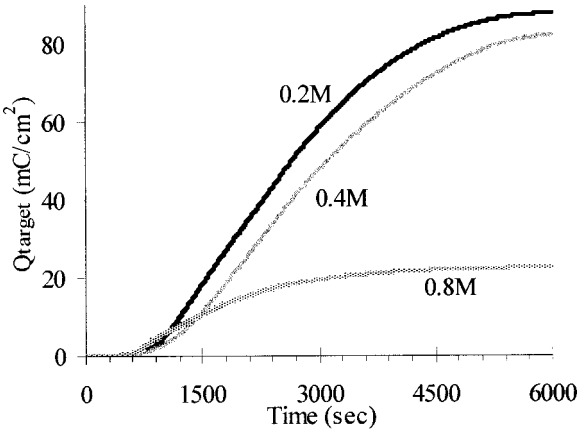

Figure 13. The deposition charge at the target electrode measured with different supporting electrolyte concentrations. The lower charge collected at the higher concentrations is attributed to the screening of the applied potential by the electrolyte. The deposition was made under illumination.

distance that is subjected to migration. Consequently, ions that are generated at a distance greater than the field penetration depth will move to the target electrode only by diffusion until they enter the migration zone. Finally, the total motion time increases, giving rise to losses due to the short lifetime of the ions.

Conclusions

A layer of the organic semiconductor (OSC) PPEI was deposited electrochemically through the neutralization of PPEI ions. The PPEI was ionized into solution during the deposition process. This new deposition method enables the formation of a high surface area OSC electrode for efficient charge transport at high optical densities.

The deposition begins with the formation of a thin layer of insulating PPEI and proceeds through weak points in the film-forming crystals along the conductive axis of the PPEI crystals. The weak points are believed to result from doping of the layer. The doping level is higher when the electrode is illuminated during the deposition of the initial thin layer. The efficiency of the deposition is affected by three parameters, one, the distance between the source and the target electrodes; two, the deposition overpotential; and three, the supporting electrolyte concentration. These parameters provide a control of the PPEI layer properties primarily regarding the amount of material deposited. Additional experiments regarding the influence of the ion charge and deposition rate are under review.

Acknowledgment

The authors acknowledge the Israel Ministry of Science (MOS) for supporting this work.

Bar-Ilan University assisted in meeting the publicaton costs of this article.

References

1. G. Tamizhmani, J. P. Dodelet, R. Cote, and D. Gravel, *Chem. Mater.*, **3**, 1046 (1991).
2. N. R. Armstrong, *J. Porphyr. Phthalocyanines*, **4**, 414 (2000).
3. M. Schneider, J. Hagen, D. Haarer, and K. Mullen, *Adv. Mater.*, **12**, 351 (2000).
4. M. Yamaguchi and T. Nagatomo, *Thin Solid Films*, **363**, 21 (2000).
5. G. Gu, G. Parthasarathy, P. E. Burrows, P. Tian, I. G. Hill, A. Kahn, and S. R. Forrest, *J. Appl. Phys.*, **86**, 4067 (1999).
6. K. Y. Law, *Chem. Rev.*, **93**, 449 (1993).
7. J. Janata, *Anal. Chem.*, **64**, R196 (1992).
8. B. A. Gregg, *Chem. Phys. Lett.*, **258**, 376 (1996).
9. C. Videlot, D. Fichou, and F. Garnier, *J. Chim. Phys. Phys.-Chim. Biol.*, **95**, 1335 (1998).
10. H. Yanagi, N. Tamura, S. Taira, H. Furuta, S. Douko, G. Schnurpfeil, and D. Wohrle, *Mol. Cryst. Liq. Cryst. Sci. Technol., Sect. A*, **267**, 435 (1995).
11. S. R. Forrest, *Chem. Rev.*, **97**, 1793 (1997).
12. J. J. Dittmer, R. Lazzaroni, P. Leclere, P. Moretti, M. Granstrom, K. Petritsch, E. A. Marseglia, R. H. Friend, J. L. Bredas, H. Rost, and A. B. Holmes, *Sol. Energy Mater. Sol. Cells*, **61**, 53 (2000).
13. M. Hiramoto, H. Fukusumi, and M. Yokoyama, *Appl. Phys. Lett.*, **61**, 2580 (1992).
14. K. Petritsch, J. J. Dittmer, E. A. Marseglia, R. H. Friend, A. Lux, G. G. Rozenberg, S. C. Moratti, and A. B. Holmes, *Sol. Energy Mater. Sol. Cells*, **61**, 63 (2000).
15. Y. Yuan, B. A. Gregg, and M. F. Lawrence, *J. Mater. Res.*, **15**, 2494 (2000).
16. A. M. van de Craats, J. M. Warman, P. Schlichting, U. Rohr, Y. Geerts, and K. Mullen, *Synth. Met.*, **102**, 1550 (1999).
17. G. Horowitz, F. Kouki, P. Spearman, D. Fichou, C. Nogues, X. Pan, and F. Garnier, *Adv. Mater.*, **8**, 242 (1996).
18. S. R. Forrest, L. Y. Leu, F. F. So, and W. Y. Yoon, *J. Appl. Phys.*, **66**, 5908 (1989).
19. B. O'Regan and M. Gratzel, *Nature (London)*, **353**, 737 (1991).
20. S. K. Lee, Y. B. Zu, A. Herrmann, Y. Geerts, K. Mullen, and A. J. Bard, *J. Am. Chem. Soc.*, **121**, 3513 (1999).
21. B. A. Gregg and R. A. Cormier, *J. Phys. Chem. B*, **102**, 9952 (1998).
22. A. J. Makinen, A. R. Melnyk, S. Schoemann, R. L. Headrick, and Y. L. Gao, *Phys. Rev. B*, **60**, 14683 (1999).
23. J. C. Conboy, E. J. C. Olson, D. M. Adams, J. Kerimo, A. Zaban, B. A. Gregg, and P. F. Barbara, *J. Phys. Chem. B*, **102**, 4516 (1998).
24. A. Zaban and Y. Diamant, *J. Phys. Chem. B*, **104**, 10043 (2000).
25. B. A. Gregg, *J. Phys. Chem. B*, **100**, 852 (1996).
26. W. Lu, J. P. Gao, Z. Y. Wang, Y. Qi, G. G. Sacripante, J. D. Duff, and P. R. Sundararajan, *Macromolecules*, **32**, 8880 (1999).
27. J. R. Ostrick, A. Dodabalapur, L. Torsi, A. J. Lovinger, E. W. Kwock, T. M. Miller, M. Galvin, M. Berggren, and H. E. Katz, *J. Appl. Phys.*, **81**, 6804 (1997).